Surface Review and Letters, Vol. 5, No. 6 (1998) 1241–1248

ELEMENT-SELECTIVE MAGNETIC IMAGING IN EXCHANGE-COUPLED SYSTEMS BY MAGNETIC PHOTOEMISSION MICROSCOPY

W. KUCH, R. FRÖMTER, J. GILLES and D. HARTMANN
Max-Planck-Institut für Mikrostrukturphysik, Weinberg 2, D-06120 Halle, Germany

CH. ZIETHEN, C. M. SCHNEIDER* and G. SCHÖNHENSE
Institut für Physik, Johannes Gutenberg-Universität Mainz, Staudingerweg 7, D-55099 Mainz, Germany

W. SWIECH
Materials Research Laboratory, University of Illinois at Urbana-Champaign, Urbana, IL 61801, USA

J. KIRSCHNER
Max-Planck-Institut für Mikrostrukturphysik, Weinberg 2, D-06120 Halle, Germany

Received 16 June 1998

We have used a photoemission microscope to obtain element-resolved magnetic contrast in stacked magnetic thin film systems. Magnetic information is thereby provided by X-ray magnetic circular dichroism. Elemental sensitivity, which is crucial for studying magnetic coupling phenomena in systems with several different layers, is achieved by tuning the energy of the illuminating photons to atomic absorption edges. We present measurements of a Ni-coated Co micropattern on Cu(001), and a wedged Co/Cr/Fe(001) sample. In the former sample the Ni magnetization is seen to follow the magnetization of the Co pattern, thereby changing from an out-of-plane easy axis in areas without underlying Co to in-plane on top of the Co microstructures. In the latter a reversal of the exchange coupling of the Co layer to the Fe magnetization is observed when the Cr layer thickness exceeds approximately two monolayers. A small net magnetic moment is also observed in the Cr spacer layer, which follows in sign the Co magnetization at the reversal of the exchange coupling. This finding is discussed in terms of interface roughness or interdiffusion.

The recent interest in magnetic coupling phenomena of ultrathin films has been nourished both by fundamental questions and by the prospect of commercial applications. On the fundamental side the striving for basic knowledge of the magnetic exchange coupling[1] of two magnetic layers across a nonmagnetic spacer layer and its dependence on the thicknesses and compositions of the film has challenged experimentalists[2–7] as well as theoreticians.[8–12] Technologically such systems have attracted considerable attention since the discovery of the connection of the magnetic exchange coupling with large changes in the electrical resistance.[13–15] This so-called giant magnetoresistance (GMR) effect offers a huge potential for applications, primarily in data storage.[16] Devices based on the GMR effect for reading magnetic information from a storage disk allow a hitherto unattainable reduction in size, and thus promise

*Present address: Institut für Festkörper and Werkstofforschung, Postfach 27 00 16, D-01171 Dresden, Germany

to keep pace with the fast increase in areal storage density.[17] Arrays of magnetoresistive submicrometer devices are being developed for random access memory application.[18] In each case the magnetic and resistive properties of the commercially interesting devices are tailored to meet specific requirements by combining a variety of functional layers, which act as seed, buffer, lead, spacer, or pinning layers. For the study of such systems, the size of which is reaching down into the micromagnetics regime, the requirement of probing magnetic information with both spatial *and* elemental resolution becomes obvious. Combining photoelectron emission microscopy (PEEM) with excitation by circularly polarized soft X-ray synchrotron radiation (X-PEEM), tuned to atomic absorption edges, can offer the desired spatially and elementally resolved magnetic information.[19,20] Magnetic contrast is thereby provided by X-ray magnetic circular dichroism (XMCD).[21–23] XMCD is the difference in absorption cross section upon helicity reversal, and depends on the relative orientation of local sample magnetization and incident light. The absorption of X-ray photons manifests itself in the emission of electrons, which are imaged by the PEEM. The exponential attenuation length of the probed electrons is thereby about 20 Å in the case of 3*d* metals.[24] Scanning the photon energy across an absorption edge and recording total electron yield spectra with the PEEM allows one even to extract quantitative information about magnetic properties with spatial resolution by applying so-called sum rules, which have been proposed for the analysis of XMCD absorption spectra.[25]

In this contribution we describe the application of a newly designed photoemission microscope (Focus IS-PEEM, with a routinely achieved resolution in threshold photoemission that is better than 30 nm) to demonstrate the versatility of this approach for the element-selective study of magnetic coupling phenomena of micropatterned structures and buried layers. By examining the magnetic domain structure of a Ni-coated artificially microstructured Co ultrathin film on Cu(001), we will show how the elemental resolution helps to obtain magnetic information also from subsurface layers, as long as the thickness of the cap layers does not exceed a few times the probing depth. A common means of conveniently studying the thickness dependence of thin film properties is to image their spatial distribution on wedge-shaped samples. We will present an investigation of the magnetic exchange coupling between a Co ultrathin film and an Fe(001) substrate across a wedged Cr interlayer. The elemental sensitivity and the ability to access also buried layers allows one not only to image the magnetization direction in the top magnetic Co layer with respect to the Fe substrate, but also the residual net magnetic signal of the Cr spacer layer.

A schematic setup of the photoelectron emission microscope is shown in Fig. 1. A more detailed description of the instrument has already been published elsewhere,[20] so here only a brief description is given. The instrument is a three-lens electrostatic straight optical axis microscope with an integral sample stage and a variable contrast aperture. An electrostatic octupole stigmator in the back focal plane of the objective lens allows correction of astigmatism and alignment of the optical axis in any rotational direction. The image is magnified by a

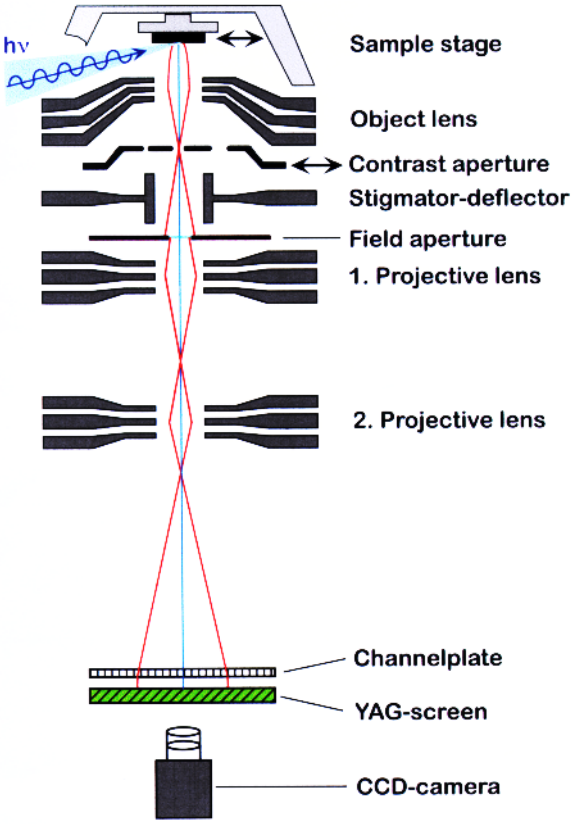

Fig. 1. Schematic setup of the photoelectron emission microscope (Focus IS-PEEM) with an integral sample stage and a variable contrast aperture.

two-stage projective lens system, intensified by a multichannel plate, and converted into visible light by means of a scintillator crystal. The image is then computer-recorded with 16-bit intensity resolution with a Peltier-cooled slow scan CCD camera. Constrast apertures with different diameters can be selected *in situ* by x–y movement of a multiaperture mount. For the measurements presented here a 200 μm diameter aperture was used. Experiments were performed at the beamline PM 3 at the Berlin synchrotron radiation source (BESSY), and at the beamline ID 12B of the European Synchrotron Radiation Facility (ESRF) in Grenoble. At BESSY light emitted from a bending magnet was accepted 0.3 mrad above and below the storage ring orbit, resulting in an estimated degree of circular polarization of about 40% at photon energies between 800 and 1000 eV.[26] At the ESRF the helicity of the helical undulator of the beamline was switched to deliver right and left circularly polarized light of more than 85% polarization.[27] The light was incident with an angle of 25° to the sample surface, thus allowing the imaging of both magnetization components for in-plane and perpendicular magnetization. The element-resolved magnetic contrst is achieved by subtracting images recorded for both helicities of the exciting light at the L_3 absorption edges of Cr, Fe, Co and Ni at photon energies of 575, 707, 779 and 855 eV, respectively. To correct for imperfections of the imaging system and suppress the topographical and work function contrast, asymmetry images are reported, which result from normalizing this difference by the sum. Film preparation and image acquisition were performed in a vacuum better than 5×10^{-8} Pa.

Figure 2(a) shows a sketch of the micropatterned epitaxial sample. Fifteen monolayers (ML) of Co were electron-beam-evaporated through a copper grid mask comprising an array of 8×8 μm^2 square apertures with 12 μm period located about 100 μm in front of a clean Cu(001) substrate surface. This resulted in the Co micropattern as schematically depicted. The azimuthal orientation of the Co squares with respect to the crystallographic orientation of the Cu substrate and the direction of light incidence is indicated in Fig. 2(b). After removal of the grid, the Co structures were coated with 8 ML of Ni. Both deposition steps were done at room temperature, with evaporation rates of about 0.7 ML/min (Co) and 0.2 ML/min (Ni). To illustrate better the influence of the Co structures on the magnetic behavior of the Ni film, the images presented in Fig. 2 have been recorded at the edge of the mask, which leaves an area free of Co on the right hand side of the images.

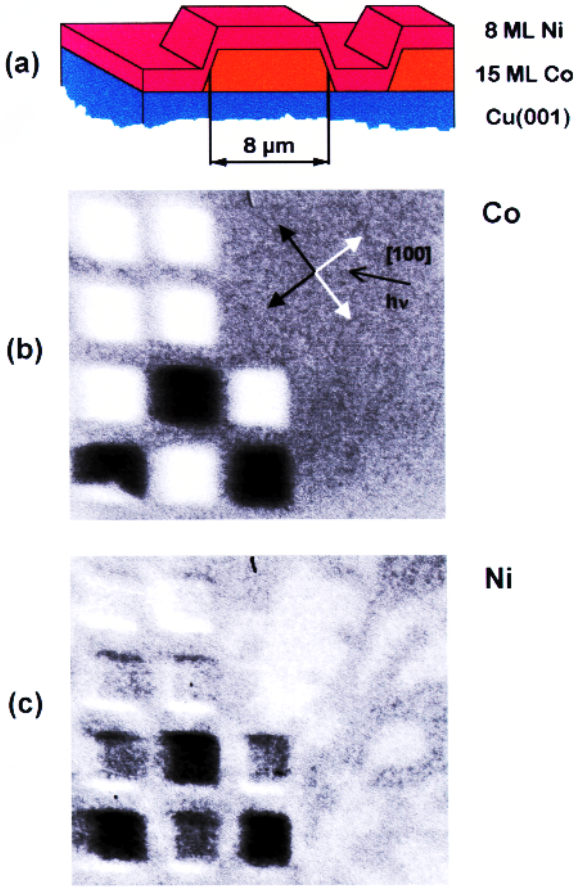

Fig. 2. (a) Sketch of the micropatterned epitaxial Ni/Co film. An array of 15-ML-thick 8×8 μm^2 Co squares with a 12 μm period on top of Cu(001) is coated with 8 ML of Ni. (b) Element-specific asymmetry image of the micropatterned Ni/Co film, recorded at the Co L_3 edge. Co squares are present only on the left hand side of the image. Different gray shades correspond to different projections of the magnetization direction onto the direction of the incoming light. The arrows suggest possible in-plane orientations of the Co magnetization. (c) Same as (b), but recorded at the Ni L_3 edge. Rounded out-of-plane domains are observed off the Co squares; on top of the Co squares the Ni magnetization follows that of the Co and is in-plane. The inset shows the geometry of the experiment. Because of the oblique incidence angle both in-plane and out-of-plane magnetization directions contribution to the magnetic contrast.

Figures 2(b) and 2(c) show a typical domain structure of this film in the as-grown state at the Co and Ni L_3 edges, respectively. The images were taken at BESSY at room temperature. The settings of the microscope were chosen to give a spatial resolution of about 500 nm; the monochromator exit slit was set to 200 μm, corresponding to a resolving power of about 200. This resulted in an exposure time of 10 min for each helicity. The spatially resolved asymmetry in the total electron emission intensity, which is a measure for the magnetization component in direction of the light incidence, is reproduced in Figs. 2(b) and 2(c) in a gray scale. Dark areas have a positive magnetization component in the direction of the incident light, bright areas a negative. Figure 2(b) shows the image taken at the Co L_3 edge, i.e seen through the Ni layer. Only three different gray scale levels are present in this image. The intermediate gray level outside the Co squares corresponds to zero asymmetry; bright and dark areas on the Co structures represent two opposite projections of the magnetization onto the direction of light incidence.

In films with a fourfold in-plane rotational symmetry one would expect four equivalent easy axes of in-plane magnetization. In epitaxial Co films on Cu(001) the easy axis was found to be along the substrate [110] azimuth.[28] In our experiment the substrate was aligned with its in-plane [100] crystallographic direction in the direction of the incident X-rays. A spontaneous magnetization of the Co squares along the four $\langle 110 \rangle$ directions would thus result in equal projections of either two of these easy axes along the light incidence. This would lead to the observation of only two different asymmetries in the experiment. The experimental finding is thus compatible with the Co structures magnetized in one of these fourfold crystallographic axes, which are indicated by two white and two black arrows in Fig. 2(b).

Another explanation for the appearance of only two different asymmetries in the present case could be the presence of a uniaxial in-plane anisotropy, aligning the magnetization along one principal axis. Such a uniaxial anisotropy could be induced, for example, by atomic steps in the substrate due to a miscut.[29] In the demagnetized state this would result in only two (opposite) directions of the magnetization, leading also to the observed gray tones. To unequivocally determine the direction of magnetization one would have to rotate the sample *in situ* around its azimuth. This is, unfortunately, not possible with the instrument in the present state. Work is in progress, however, to provide such a sample azimuthal rotation inside the microscope for future studies.

Figure 2(c) shows the asymmetry image recorded at the same spot of the sample at the Ni L_3 edge. The direction of light incidence is the same as in Fig. 2(b). The magnetic contrast at the positions of the underlying Co squares resembles the contrast observed at the Co L_3 edge. The bright and dark contrast right at the lower and upper edges of the squares, respectively, are an artifact due to a slight vertical sample drifft between the acquisition of the two images for opposite light helicity. In the Ni image additional domains are also observed in the region outside the Co structures, where the 8 ML Ni film sits directly on the Cu substrate. These domains exhibit a rounded shape, and a lower asymmetry difference between dark and bright. It is known that in ultrathin Ni films on Cu(001) the easy axis of magnetization turns from in-plane to perpendicular with increasing Ni thickness between 7 and 10 ML, and again to in-plane between 56 and 75 ML.[30,31] The Ni thickness of the first spin reorientation transition further varies slightly for different substrate temperatures during Ni deposition.[32] From the thickness of the Ni film, the rounded shape of the domains (which is indicative of a perpendicular magnetization), the knowledge from the literature, and our own investigations of Ni/Cu(001), we conclude that the Ni magnetization in the regions outside the Co squares is perpendicular to the film plane. On the Co squares the Ni magnetization is ferromagnetically aligned with the Co magnetization, which, due to the strong magnetostatic shape anisotropy of 15 ML Co, lies in the film plane. The inset of Fig. 2(c) shows the geometry of the light incidence in the present measurements. As already mentioned, both in-plane and out-of-plane magnetization directions contribute to the magnetic signal. Because of the incidence angle of 25° to the sample surface the projection of the magnetization onto the light helicity is lower in the case of perpendicular magnetization, which leads to the lower asymmetry difference between oppositely magnetized domains outside the Co squares. We therefore conclude from the images shown in Fig. 2 that the film undergoes a spin reorientation

transition from perpendicular to in-plane induced by the underlying Co.

It should be noted that the gray scales for the magnetic contrast in Figs. 2(b) and 2(c) are not identical, but are scaled to show the full range of resulting asymmetry values present in each image. Since raw images acquired at the maximum of the Ni L_3 absorption were used to calculate the asymmetry, and no background correction was performed, the tail of the energetically lower-lying Co $L_{2,3}$ absorption contributes to the Ni image, and induces the artifactual offset of the Ni asymmetry on top of the Co squares with respect to the area beside the Co squares, as is seen in Fig. 2(c). Although the Co signal is attenuated upon transmission through the Ni overlayer, it exhibits in the present case still the better signal-to-noise ratio at identical exposure time, because of the smaller XMCD asymmetry of Ni compared to Co.

The random pattern of dark and bright Co squares indicates that there is little or no interaction between different squares. Horizontally patterned films appear technologically promising, because of the additional control of magnetic properties by the design of the pattern.[33] With decreasing separation between the structures of such patterns, magnetic interactions between neighboring structures become increasingly important. Further work is in progress to image significantly smaller patterns with improved lateral resolution, and to study their properties and lateral interaction.

Figure 3(a) is a sketch of the Co/Cr/Fe sample used to study the magnetic exchange coupling between Fe and Co across a Cr spacer layer. On an Fe(001) whisker (300 μm width) a Cr wedge with a slope of ≈ 8 ML/mm was deposited by positioning a mask 0.7 mm in front of the sample and rocking the joint mask sample assembly by $\pm 17^\circ$ during evaporation. After deposition of the Cr wedge it was completely covered with 5 ML Co. Both deposition steps were done at 500 K, with evaporation rates of about 0.1 ML/min (Cr) and 0.5 ML/min (Co). Figures 3(b)–3(d) show asymmetry images recorded at the ESRF at room temperature from the same area of the sample but with the photon energy turned to the Fe, Co and Cr L_3 edges, respectively. In these images the light was incident from the left, along the wedge gradient. The settings of the

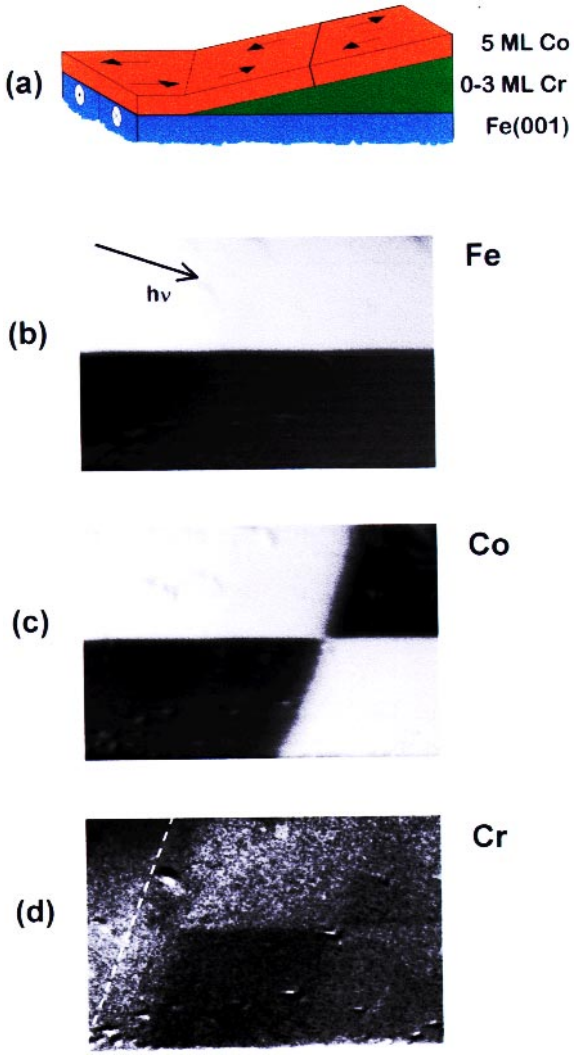

Fig. 3. (a) Sketch of the wedge-shaped Co/Cr layer on an Fe(001) whisker. A 0–3 ML Cr wedge is covered with 5 ML Co. Arrows indicate the direction of magnetization in the substrate and in the Co overlayers as found from the element-resolved magnetic domain images (b)–(d). (b) Element-specific asymmetry image recorded at the Fe L_3 edge. The Fe substrate exhibits a simple domain configuration of two oppositely magnetized domains aligned parallel to the whisker. (c) Element-specific asymmetry image recorded at the Co L_3 edge. The orientation of the Cr wedge is tilted by 19° with respect to the Fe whisker; the Cr thickness increases from left to right. The Co magnetization follows that of the Fe substrate up to a Cr coverage of ≈ 2 ML; at higher Cr film thicknesses antiferromagnetic coupling is observed. (d) Element-specific asymmetry image recorded at the Cr L_3 edge. The onset of the Cr wedge is indicated by the white broken line. The Cr magnetization follows that of the Co cover layer, except at the very lowest Cr coverages (≤ 0.3 ML), where the Cr magnetization is opposite to that of Fe and Co.

photoemission microscope were adjusted to enable the imaging of a relatively large area of the sample. This is achieved by using low extraction fields ($\approx$ 200 V, survey mode). A lateral resolution of about 1 μm and a field of view of more than 700 μm are the consequences. The exposure time for all of these images was only about 5 min for each helicity, thanks to the high brightness of the insertion device.

Figure 3(b) shows the asymmetry at the Fe L_3 edge, representing the Fe substrate magnetization seen through the Cr and Co layers. It consists of two oppositely magnetized domains aligned alongside the whisker, which is parallel to the horizontal edges of the image. The magnetization of these domains is indicated on the left hand edge of the sketch in Fig. 3(a). Bright areas correspond to a magnetization orientation opposite to the direction of the incident light, and dark areas to a magnetization along the light incidence. Such a simple domain configuration is often encountered in Fe whiskers, and is very convenient for imaging magnetic coupling in wedge-shaped overlayers.[6,7,34]

In Fig. 3(c) the corresponding image acquired at the Co L_3 edge is reproduced. The orientation of the Cr wedge is such that it increases from upper left to lower right, with a tilt angle of 19° with respect to the Fe whisker, as indicated schematically in Fig. 3(a). The highest Cr thickness in the lower right hand corner is about 3 ML. Comparing panels (b) and (c), one sees that at low Cr thickness the Co magnetization follows that of the Fe substrate, i.e the Co is coupled ferromagnetically to the Fe. For Cr thicknesses above $\approx$ 2 ML the magnetic contrast in the Co image is reversed with respect to the Fe image; Co hence displays an antiferromagnetic coupling to the Fe substrate at these Cr thicknesses. At the transition from ferromagnetic to antiferromagnetic coupling at 2 ML Cr coverage, a small region with an intermediate gray scale contrast is observed. This could be due to a simultaneous presence of ferromagnetic and antiferromagnetic coupling in that region, or to a biquadratic coupling behavior, which would result in a 90° rotation of the Co magnetization.[36] From the present measurements we cannot distinguish between these two possibilities.

The bottommost panel [Fig. 3(d)] shows the image recorded at the Cr L_3 edge. As mentioned before, a particular advantage of the technique lies in the combination of element selectivity and access to buried layers. This makes it possible to study the residual ferromagnetic ordering of the Cr wedge, induced by the adjacent Fe and Co magnetic layers. Figures 3(d) shows that there is indeed a net ferromagnetic moment also in the Cr layer. The onset of the Cr wedge is indicated by the white broken line. Left of that line no Cr was deposited. The Cr magnetization follows that of the Co cover layer, with a darker constrast on the bottom half at the center of the image, and a darker area also on the upper right hand side. Only at the lowest Cr coverages below $\approx$ 0.3 ML, just right of the broken line, does the Cr magnetization seem to be opposite to that of Fe and Co. We observe a similar behavior on submonolayer Cr wedges on Fe(001) without additional overlayers, in the cases where the Cr is deposited at room temperature or slightly elevated temperatures. The temperature dependence of this effect points towards an important role of the Fe/Cr interface, and will be discussed in a forthcoming publication.[37] At this point we would like to emphasize again that elemental selectivity is an absolutely necessary prerequisite for studying the coupling behavior of submonolayer coverages on a ferromagnetic surface.

The Cr thickness where the antiferromagnetic exchange coupling is first observed (2 ML in Co/Cr/Fe) is lower than that of Fe/Cr/Fe (4–5 ML).[6,34] Whereas the period of the oscillation in the interlayer exchange coupling depends only on the nonferromagnetic interlayer material, different magnetic layers may influence the phase.[5,12] The difference in the Cr switching thickness could thus be attributed to a phase shift in the oscillations in the exchange coupling due to the different matching of the electronic states of Co to Cr compared to Fe and Cr. A significant influence of the amount of interface intermixing on the occurrence of the antifferromagnetic interlayer coupling[35] may also play a role.

The asymmetry contrast at the Cr L_3 edge [Fig. 3(d)] is only between 0.2 and 0.5% compared to about 20% at the Fe or Co L_3 edges [Figs. 3(b) and 3(c), respectively]. This indicates that the total net moment of the Cr layer is much lower than the Fe or Co moments. Furthermore, the contrast is significantly weaker in the region of antiferromagnetic exchange coupling compared to the region of ferromagnetic alignment between Fe and Co. On the right hand side of Fig. 3(d) the domain boundary between the upper and lower Fe domains is hardly discernible

in the Cr signal. If we assume that the apparent ferromagnetic moment in the Cr is primarily induced at the interfaces, the parallel alignment in the region of ferromagnetic exchange coupling points towards a net ferromagnetic contribution at both the Fe/Cr and Co/Cr interfaces. Assuming further that no change in these interface contributions occurs at the Cr thickness at which the exchange coupling changes from ferromagnetic to antiferomagnetic, the two interface contributions would tend to cancel out in the antiferromagnetically coupled region. This would explain the drop in asymmetry contrast above 2 ML Cr thickness. The residual Cr magnetism above 2 ML is oriented along the Co magnetization direction. In the above argumentation this leads to the conclusion that the Co/Cr interface contribution outweighs the Fe/Cr contribution to the Cr net moment. This could be attributed to interface roughness, which probably is higher between Cr and Co because of different roughness at the upper and lower Cr interfaces in the film growth at 500 K.[38] We note that due to the limited probing depth the Co/Cr interface has a somewhat higher weight in the images than the Fe/Cr interface; at 2 ML Cr thickness, however, this leaves only a less than 15% difference between the two interfaces, and the drop in asymmetry connected the effect of different weight alone should be much bigger.

In conclusion, we have demonstrated in this contribution how magnetic domain imaging using circularly polarized synchrotron radiation with a PEEM can be used to study magnetic coupling in a laterally resolved way. A specific feature of this approach is the selective mapping of buried layers and microstructures. The magnetic behavior of an array of Co microstructures coated with a perpendicularly magnetized Ni film was imaged. The interlayer exchange coupling between Co and Fe across Cr was investigated by imaging a wedged Co/Cr/Fe sample. By tuning the photon energy to the Co L_3 absorption edge the sign of the exchange coupling could be determined, which was found to change from ferromagnetic to antiferromagnetic at 2 ML Cr thickness. Besides, it was possible to detect a ferromagnetic signal from the Cr spacer layer. This signal follows the Co magnetization except for Cr coverages below $\approx$ 0.3 ML. The smaller Cr asymmetry in the region of antiferromagnetic coupling at Cr thickness between 2 and 3 ML compared to Cr below 2 ML suggests that the observed Cr ferromagnetism is due to ferromagnetic coupling at the interfaces. Future work will be devoted to clarifying the role of interface quality and its dependence on growth temperature in the interface coupling of Cr to ferromagnetic materials.

Acknowledgments

We thank the BESSY and ESRF staff for their help during the experiments, especially M. Finazzi and N. B. Brookes (ESRF) and H. Gundlach (BESSY). We also thank B. Zada for her expert technical support. Funding by the BMBF under contracts. 05644EFA5 and 05621UMA2 is gratefully acknowledged. W. S. thanks the U.S. Department of Energy, Division of Materials Sciences, for travel support under award DEFG 02-96 ER45439.

References

1. P. Grünberg, R. Schreiber, Y. Pang, M. B. Brodsky and H. Sowers, *Phys. Rev. Lett.* **57**, 2442 (1986).
2. S. S. P. Parkin, N. More and K. P. Roche, *Phys. Rev. Lett.* **64**, 2304 (1990); S. S. P. Parkin, *Phys. Rev. Lett.* **67**, 3598 (1991).
3. A. Cebollada, R. Miranda, C. M. Schneider, P. Schuster and J. Kirschner, *J. Magn. Magn. Mater.* **102**, 25 (1991).
4. P. J. H. Bloemen, M. T. Johnson, M. T. H. van de Vost, R. Coehoorn, J. J. de Vries, R. Jungblut, J. aan de Stegge, A. Reinders and W. J. M. de Jonge, *Phys. Rev. Lett.* **72**, 764 (1994).
5. M. T. Johnson, M. T. H. van de Vorst, P. J. H. Bloemen, R. Coehoorn, A. Reinders, J. aan de Stegge and R. Jungblut, *Phys. Rev. Lett.* **75**, 4686 (1995).
6. J. Unguris, R. J. Celotta and D. T. Pierce, *Phys. Rev. Lett.* **67**, 140 (1991).
7. J Unguris, R. J. Celotta and D. T. Pierce, *Phys. Rev. Lett.* **79**, 2734 (1997).
8. D. Edwards and J. Mathon, *J. Magn. Magn. Mater.* **93**, 85 (1991); J. Mathon, M. Villeret, A Umerski, R. B. Muniz, J. d'Albuquerque e Castro, and D. M. Edwards, *Phys. Rev.* **B56**, 11797 (1997).
9. M. D. Stiles, *Phys. Rev.* **B48**, 7238 (1993).
10. P. Bruno, *Phys. Rev.* **B52**, 411 (1995).
11. P. B. Allen, *Solid State Commun.* **102**, 127 (1997), and references therein.
12. J. Kudrnovský, V. Drchal, R. Coehoorn, M. Šob and P. Weinberger, *Phys. Rev. Lett.* **78**, 358 (1997).
13. M. N. Baibich, J. M. Broto, A. Fert, F. Nguyen van Dau, F. Petroff, P. Eitenne, G. Creuzet, A Friederich and J. Chazelas, *Phys. Rev. Lett.* **61**, 2472 (1988).
14. G. Binasch, P. Grünberg, F. Saurenbach and W. Zinn, *Phys. Rev.* **B39**, 4828 (1989).

15. S. S. P. Parkin, R. Bhadra and K. P. Roche, *Phys. Rev. Lett.* **66**, 2152 (1991).
16. J. A. Brug, T. C. Anthony and J. H. Nickel, *MRS Bulletin*, Sept. 1996, p. 23.
17. J. L. Simonds, *Physics Today*, Apr. 1995, p. 26.
18. G. J. Gallagher, J. H. Kaufman, S. S. P. Parkin and R. E. Scheuerlein, US-Patent No. 5640343.
19. J. Stöhr, Y. Wu, M. G. Samant, B. B. Hermsmeier, G. Harp, S. Koranda, D. Dunham and B. P. Tonner, *Science* **259**, 658 (1993).
20. W. Swiech, G. H. Fecher, C. Ziethen, O. Schmidt, G. Schönhense, K. Grzelakowski, C. M. Schneider, R. Frömter, H. P. Oepen and J. Kirschner, *J. Electron Spectr. Rel. Phen.* **84**, 171 (1997); C. M. Schneider, *J. Magn. Magn. Mater.* **175**, 160 (1997).
21. G. Schütz, W. Wagner, W. Wilhelm, R. Kienle, R. Zeller, R. Frahm and G. Materlik, *Phys. Rev. Lett.* **58**, 737 (1987).
22. C. T. Chen. Y. U. Idzerda, H.-J. Lin, N. V. Smith, G. Meigs, E. Chaban, G. H. Ho, E. Pellegrin and F. Sette, *Phys. Rev. Lett.* **75**, 152 (1995).
23. J. Stöhr, *J. Electron Spectr. Rel. Phen.* **75**, 253 (1995).
24. W. L. O'Brien and B. P. Tonner, *Phys Rev.* **B50**, 2963 (1994).
25. B. T. Thole, P. Carra, F. Sette and G. van der Laan, *Phys. Rev. Lett.* **68**, 1943 (1992); P. Carra, B. T. Thole, M. Altarelli and X. Wang, *ibid.* **70**, 694 (1993).
26. W. Kuch, M. Salvietti, Xingyu Gao, M.-T. Lin, M. Klaua, J. Barthel, Ch. V. Mohan and J. Kirschner, *Phys. Rev. B*, in print.
27. M. Drescher, G. Snell, U. Kleineberg, H.-J. Stock, N. Müller, U. Heinzmann and N. B. Brookes, *Rev. Sci. Instrum.* **68**, 1939 (1997).
28. C. M. Schneider, P. Bressler, P. Schuster, J. Kirschner, J. J. de Miguel, R. Miranda and S. Ferrer, *Vacuum* **41**, 503 (1990); C. M. Schneider, A. K. Schmid, P. Schuster, H. P. Oepen and J. Kirschner, in *Magnetism and Structure in Systems of Reduced Dimension*, eds. R. F. C. Farrow *et al.* (Plenum, New York, 1993).
29. A. Berger, U. Linke and H. P. Oepen, *Phys. Rev. Lett.* **68**, 839 (1992); H. P. Oepen, A. Berger, C. M. Schneider, T. Reul and J. Kirschner, *J. Magn. Magn. Mater.* **121**, 490 (1993).
30. W. L. O'Brien and B. P. Tonner, *Phys. Rev.* **B49**, 15370 (1994).
31. B. Schulz and K. Baberschke, *Phys. Rev.* **B50**, 13467 (1994).
32. M. Zheng, J. Shen, Ph. Ohresser, Ch. V. Mohan, J. Barthel and J. Kirschner, to be published.
33. C. Mathieu, C. Hartmann. M. Bauer, O. Buettner, S. Riedling, B. Roos, S. O. Demokritov, B. Hillebrands, B. Bartenlian, C. Cappert, D. Decanini, F. Rosseaux, E. Cambril, A. Müller, B. Hoffmann and U. Hartmann, *Appl. Phys. Lett.* **70**, 2912 (1997).
34. C. M. Schneider, K. Meinel, J. Kirschner, M. Neuber, V. Wilde, M. Grunze, K. Holldak, Z. Celinski and F. Baudelet, *J. Magn. Magn. Mater.* **162**, 7 (1996).
35. M. Freyss, D. Stoeffler and H. Dreyssé, *Phys. Rev.* **B56**, 6047 (1997).
36. M. Rührig, R. Schäfer, A. Hubert, R. Mosler, J. A. Wolf, S. Demokritov and P. Grünberg, *Phys. Stat. Sol. (a)* **125**, 635 (1991).
37. C. M. Schneider, R. Frömter, Ch. Ziethen, W. Swiech, W. Kuch, J. Gilles, M. Seider, G. Schönhense and J. Kirschner, to be published.
38. B. Heinrich, J. F. Cochran, D. Venus, K. Totland, C. M. Schneider and K. Myrtle, *J. Magn. Magn. Mater.* **156**, 215 (1996).